Mr Charles Jackson [1], Dr Rebecca Higginson [1], Dr Simon Hogg [1], Dr Sarah Spindler [2], Dr Chris Hamm [2], Mr Mike Spindler [2], Mr Keith Abbott [2]

The Effect of Long Term Ageing on the Autogenous Welding of Dissimilar Austenitic Stainless Steels

Abstract

Austenitic stainless steels are used extensively throughout power stations in high temperature applications such as superheater tubes and fuel rod guides. For these applications, welding is often required to join sections of components or pipes/tubes due to their large sizes and lengths.

In this paper, samples of a cast niobium stabilised stainless steel welded to a wrought 321 stainless steel were investigated. The sections were joined together using an autogenous Tungsten Inert Gas (TIG) weld. The effects of long term ageing at 750°C for up to 4000 hours have been studied. The ageing treatments were conducted in an inert atmosphere.

Compositional changes and precipitates have been investigated using SEM with EDX and EBSD analysis. Niobium dissolved completely into the weld melt however it is observed to precipitate back out during long term ageing. Titanium carbonitrides however remained intact during the welding process, creating agglomerated particles throughout the weld bead. Ageing above 100 hours causes further Nb rich MX precipitates to form, which coarsen with longer ageing times up to 4000 hours.

Key Words: Stainless Steel, EBSD, SEM, Weld, Long Term Ageing

Introduction

Most of the nuclear power currently generated in the UK is generated through the use of Advanced Gas Cooled Reactors (AGRs). Many of these have been in service for over twenty years, and have been scheduled to be decommissioned in the next decade [1]. This would be a costly and time consuming process, along with the knock-on effect of the requirement of other methods of baseline power generation throughout the UK. For these reasons, the lifespan of many of the AGRs are being extended further before decommissioning. However, the effect of these lifespan increases on the components and materials used must be understood.

Stainless steels have been used in high temperature applications for many years due to their advantageous properties such as high corrosion resistance, creep resistance and mechanical strength [2,3]. Components inside an AGR must be able to withstand temperatures up to 650°C for thousands of hours during service [2]. Along with this, they must also exhibit good corrosion resistance and maintain their mechanical properties during the high temperature exposure [2,4].

[1] Loughborough University, Epinal Way, Loughborough, Leicestershire, UK, LE11 3TU
[2] EDF Energy, Barnett Way, Barnwood, Gloucester, UK, GL4 3RS

Welding of materials is necessary in applications such as AGRs as many components are simply too large or long to be completely manufactured from one piece of material. Other joining methods such as riveting or bolts have proven to be less effective when put into service at high temperatures due to the high localised stresses these methods incur [5].

It is generally understood that materials will tend towards a form of thermodynamic equilibrium after initial manufacturing [5,6]. This tendency will be affected by thermal history and service temperatures [5–7]. Welding of materials greatly influences this process and it has not been very well researched, with only a handful of studies researching welds with austenitic 321 stainless steel [8–10].

Long term ageing of materials results in the tendency to form precipitates and secondary phases which can have both positive and negative effects on the mechanical properties of the material. For stainless steels in particular, common precipitates are MX, $M_{23}C_6$, and sigma [4]. MX precipitates are very common in stabilised stainless steels where M is usually Ti, Nb or V, and X is either C or N [4]. These are advantageous to the long term microstructural stability of these steels due to the locking effect they have on C and N. These form during initial solidification of the material and have been shown to have good high temperature properties by keeping their stability up to very long ageing times [11,12]. In stainless steels with high Cr, N and Nb, the Nb rich MX particles have been commonly observed to transform to a highly ordered, highly stable phase called the Z phase [13,14]. $M_{23}C_6$ particles are often observed after short ageing times at intergranular sites [15]. M is often Cr or Fe, which can sometimes be substituted for Mo or V [16]. These deplete the matrix of Cr and thus cause intergranular corrosion in austenitic stainless steels. Also, in high volume fractions they can cause grain boundary embrittlement due to a continuous film being formed through a network of these precipitates [16–18]. Sigma phase is a precipitate of FeCr, and often forms as intergranular particles usually under 2µm which are associated with embrittlement [19,20].

With these different factors in mind, it is important to understand the microstructural changes that occur in materials during long term ageing. This paper focusses on the weld material between a cast stainless steel with a duplex microstructure and wrought 321 austenitic stainless steel.

Experimental

The samples are cast Nb stabilised stainless steel autogenously welded to wrought 321 stainless steel. The compositions of these are shown in Table 1. There was no post weld heat treatment. Ageing of samples was carried out at 750°C in quartz glass tubes which were filled with argon to prevent any oxidation during the ageing process.

Samples were mounted into Bakelite and grinding was conducted from 220 grit, 600 grit and on to 1200 grit. Polishing was completed using a diamond suspension at 9µm particle size, 6µm and then 1µm. Etching for optical microscopy as completed using a solution of 50ml H_2O, 5ml HNO_3 and 50ml HCl. For EBSD analysis, polishing was then moved onto a 0.02µm colloidal silica polish. After colloidal silica polishing, samples were washed in an acetone filled sonic bath, and cleaned in a ZoneSEM ozone cleaner.

Optical microscopy was carried out using a Reichert MEF-3 optical microscope in the bright field (BF) setting. The samples were also imaged using a secondary electron (SE2) detector

and InLens (IL) detector on a Zeiss Leo 1530VP FEGSEM. Compositional and crystallographic information was obtained using Nordlys Electron Backscatter Diffraction (EBSD) detector and an Oxford Instruments X-Max Energy Dispersive X-ray Spectroscopy (EDS) detector.

Thermodynamic calculations were performed using Thermocalc software using the TCFE 7 database. Isothermal equilibrium calculations were carried out at 750°C. The compositions of the materials used in this experiment are shown in Table 1. The weld metal composition was obtained by averaging the compositions of the two base materials. This was also checked with EDX.

Table 1: Compositions of the base materials used in this experiment

Material	**%C**	**%Mn**	**%Si**	**%P**	**%Cu**	**%Ni**	**%Cr**
Cast	0.02	0.46	0.78	0.01	<.01	6	21.2
321	0.03	1.24	0.41	0.03	0.42	9.22	17.2
Material	**%Mo**	**%Nb**	**%Ti**	**%W**	**%Co**	**%N**	**%Fe**
Cast	0.13	0.54	0.01	0.03	0.01	0.02	bal
321	0.37	0.01	0.4	0.03	0.2	0.01	bal

Results and Discussion

Table 2 shows Thermocalc predictions using TCFE7 of the two base materials used during this experiment, and also the weld metal. The modelling predicts that the wrought 321 will be almost entirely austenitic with a small volume fraction of MX precipitates and Laves phase present. Predictions show that the cast material will exhibit substantial transformation to sigma phase during ageing, along with the delta ferrite remaining present from the original casting. The weld material takes on a small amount of sigma phase transformation which will be due to the general mixing of the two alloys. Along with this, Laves phase will also be present in the material at thermodynamic equilibrium. Despite Thermocalc predicting no BCC material being present in the weld material at 750°C, it is highly likely that upon cooling a BCC transformation will take place to form ferrite/martensite, as predicted by the DeLong calculation, discussed later in these results.

Upon conducting a DeLong calculation, the Cr_{eq} and Ni_{eq} values for the weld metal come out at 20.48 and 9.2 respectively [21]. This puts the weld metal firmly into the austenite + ferrite + martensite region of the Delong diagram. This means that whilst the Thermocalc predictions bring out no mention of any BCC phases, there is a martensitic transformation predicted under certain conditions in the weld metal [21].

Table 2: Thermocalc predictions for volume fractions of phases at thermodynamic equilibrium at 750°C

	W321	WELD	Cast
Austenite	99.478	90.407	75.658
Ferrite			6.134
(Ti,Nb)C		0.010	
Ti(C,N)	0.352	0.315	
Nb(C,N)			0.253
Laves Phase	0.171	0.509	0.394
Sigma Phase		8.758	17.422
Z Phase			0.138

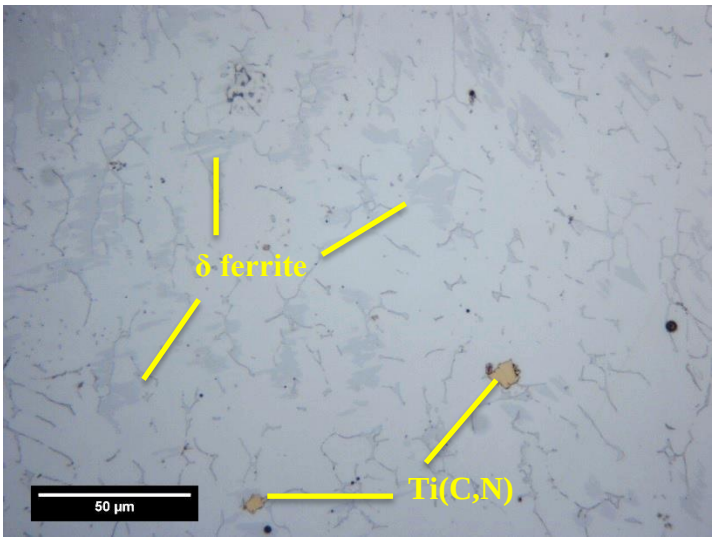

Fig.1: Optical micrograph showing the general microstructure of the unaged weld.

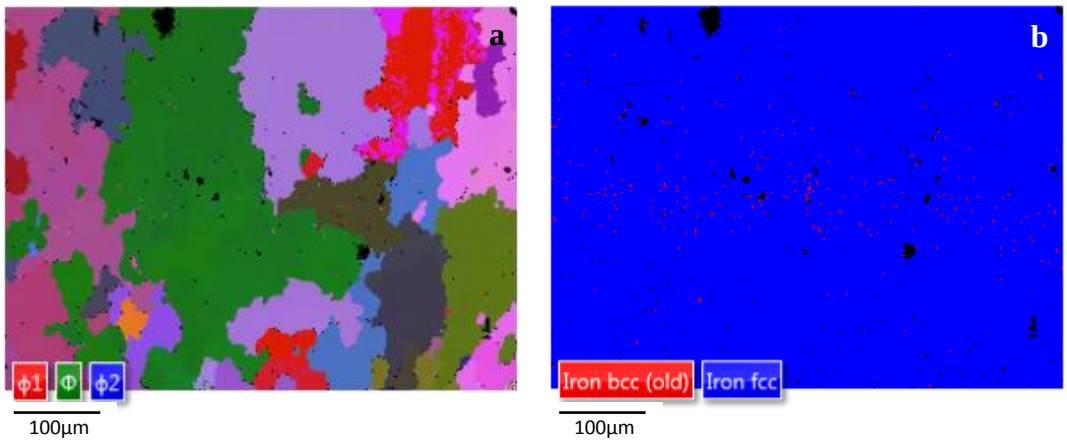

Fig.2: EBSD analysis of un-aged weld material (a) Euler color, (b) phase map

In the unaged condition, Figures 1 and 2 show the weld to have a predominantly austenitic structure with small delta ferrite regions dotted throughout. There is between 1 and 1.5% area BCC material in the weld material detected from the EBSD scans carried out. This takes the form of small lath-type sections which are labelled in Fig. 1, which correlate to the red spots observed in Fig. 2(b). The Euler figure shown in Fig. 2(a) shows the common orientation of the delta ferrite regions. The amount of BCC material does not appear to be effected by location in the weld, with weld material at the boundaries to base materials resembling the scans shown in Figure 2. Niobium-rich MX particles were not found at this stage using SEM-EDX however Ti rich particles were distributed throughout the weld. EDX analysis revealed no further localisations of elements in the unaged material. Full Nb dissolution is typical in welds however it is well noted that it rapidly precipitates during ageing [4,22]

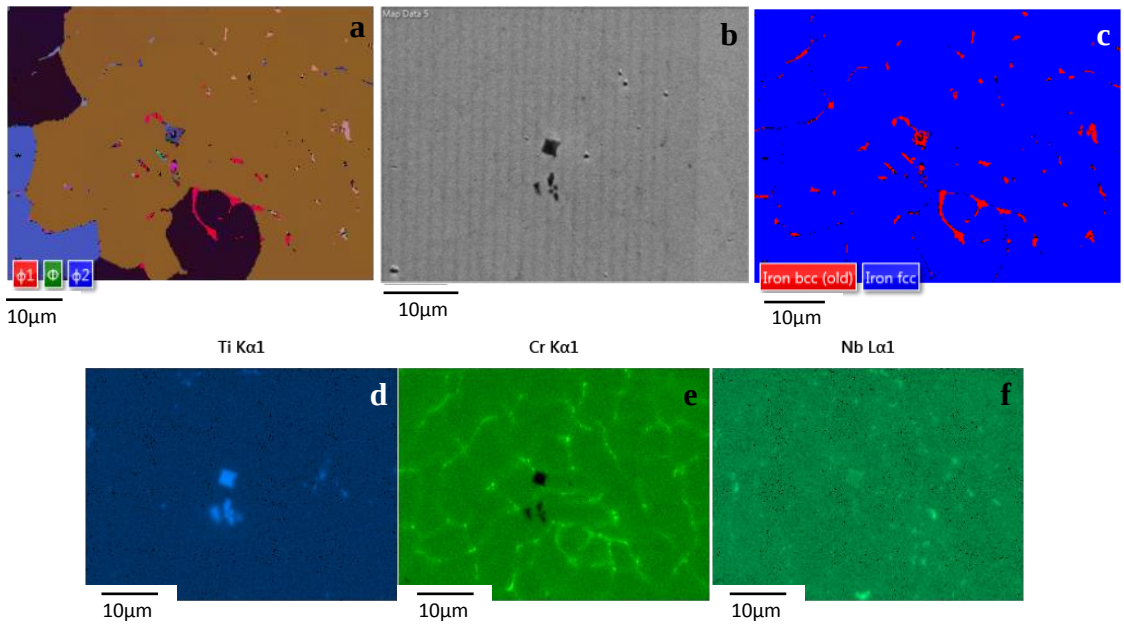

Fig.3: EBSD and EDX analysis of weld material aged for 1 hour at 750°C (a) Euler colour, (b) electron image, (c) phase distribution, (d) Ti EDX map, (e) Cr EDX map, (f) Nb EDX map.

There is no considerable increase of BCC material after 1 hour of ageing when compared to the unaged material. Fig. 3 shows the structure of the weld close to the centre of the melted zone, at a higher magnification than Fig. 2. The EDX maps in Fig. 3 confirm that the cuboidal particle in the centre of the electron image is in fact a Ti (C,N) particle, along with the other low contrast particles in the electron image with a group of large particles just

below the cube. EDX scans after 1 hour of ageing also show slight Nb enrichment of Ti-rich particles in particular, along with very small enrichments along delta ferrite regions.

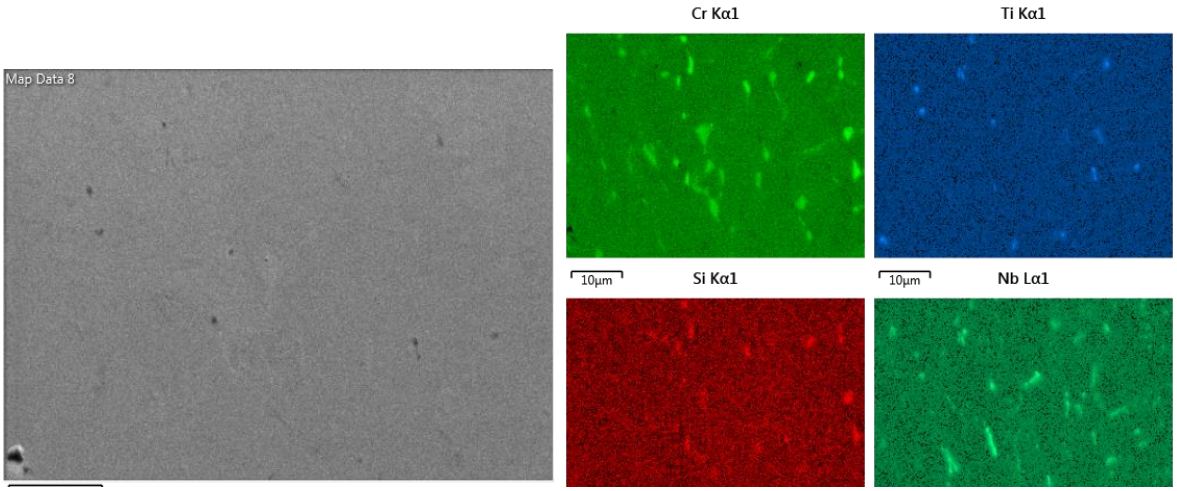

Figure 4: Electron image and EDX maps of weld metal aged for 500 hours at 750°C (a) electron image, (b) Cr EDX map, (c) Ti EDX map, (d) Si EDX map, (e) Nb EDX map.

After 500 hours of ageing at 750°C, the weld material has a slightly increased amount of BCC phase at the centre of the weld, with the amount being on average around 3%. The BCC phase increase comes in the form of a high number of small nucleation sites, developing localised regions of BCC. These particles are found to be no larger than 10um in length and appear to cluster together in groups of 5 – 10 particles. Fig. 4 shows EDX maps that indicate that Nb has now begun to form long, secondary MX particles which are between 1-2µm width but up to 10 µm in length at grain boundaries [23].

At 1000 hours of ageing, the average content of the weld material becomes difficult to obtain without a full weld scan. This is due to extensive conversion of austenite to BCC near the cast side of the weld. Fig. 5 shows an EBSD scan of the centre of the weld melt, and Fig. 5(b) an EBSD scan from the side of the weld close to the cast base material. The wrought side of the weld did not show this type of conversion to BCC at this time at 750°C. In contrast to the 500 hours aged sample, the regions of BCC material are now beginning to join together to form areas of up to 50 microns in size on the cast side of the weld. Fig. 5(b) shows this very well with the cast base material being roughly 200 µm above the top of the image shown. The amount of BCC material in Fig. 5(b) is 20%. No further particles have formed at this stage of ageing, however the Nb precipitates are larger than those found at 500 hours of ageing. Particles do not appear to have grown in size however. A similar type of conversion has been observed before in 321 austenitic stainless steel [20,24].

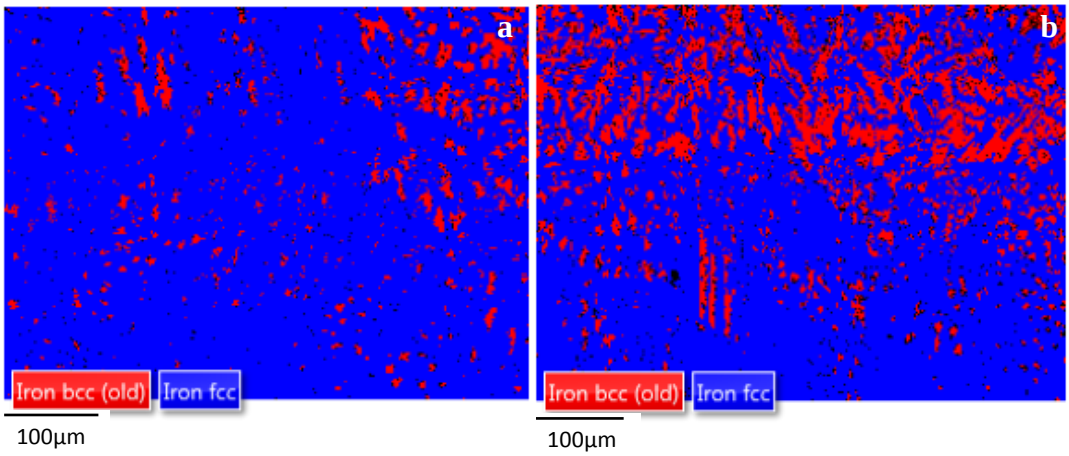

Fig.5: (a) EBSD map near the centre of weld material aged for 1000 hours at 750°C, with the weld boundary 500µm to the right. (b) EBSD map of the weld material near the border to cast base material aged for 1000 hours at 750°C, with the weld boundary 200µm above the top of the image.

After 4000 hours of ageing, the centre of the weld material remains virtually unchanged compared to 1000 hours ageing. However the area which has been advanced upon by small, localised BCC transformations on the side by the cast material has grown considerably so that now there is a large area of weld material that has transformed to BCC material. This is seen in Fig. 6 with the cast base material being roughly 500µm to the right of the image. The wrought side of the material has also begun to transform, with long columnar BCC plates becoming apparent which were not seen at any other ageing times in this experiment. This is seen in Fig. 7 with the wrought base material being roughly 200µm above the image. No new particles were discovered using SEM-EDX. Figure 7 shows the columnar shape taken by the BCC phase in the weld metal after 4000 hours ageing, which is vastly different to that of the weld metal near the cast base material. The Euler colour (Figure 7c) also shows a difference in the general form taken by the weld material in this part of the weld, which could have an effect on the growth characteristics of the BCC phase.

Thermocalc predicted no BCC material in the weld, so the BCC transformation during later ageing times is somewhat unexpected. The BCC phase transformation also relies on element diffusion, due to the reliance on close proximity to the point where the weld joins on to bulk material, along with the appearance of growing outwards from this point. However the BCC transformation is particularly unexpected within the side of the weld which joins on to the wrought base material, this was fully austenitic in the as-received state. However there are reports of ferritic transformations in 321 austenitic stainless steel by Green *et al*. [20,24]. The BCC transformation observed in the wrought side of the weld takes the same appearance as that in the literature [20,24], while the cast side globular transformation has not been found elsewhere after long term ageing.

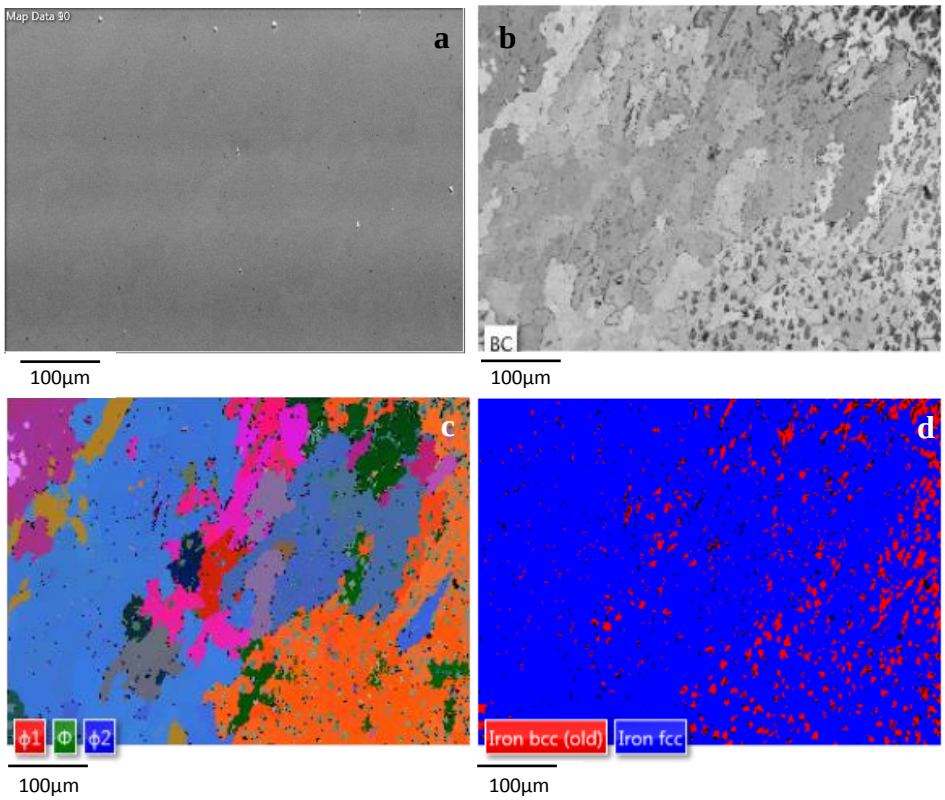

Fig.6: EBSD analysis of weld material close to the border of cast base material aged for 4000 hours at 750°C. (a) SEM image, (b) band contrast, (c) Euler colour, (d) phase distribution.

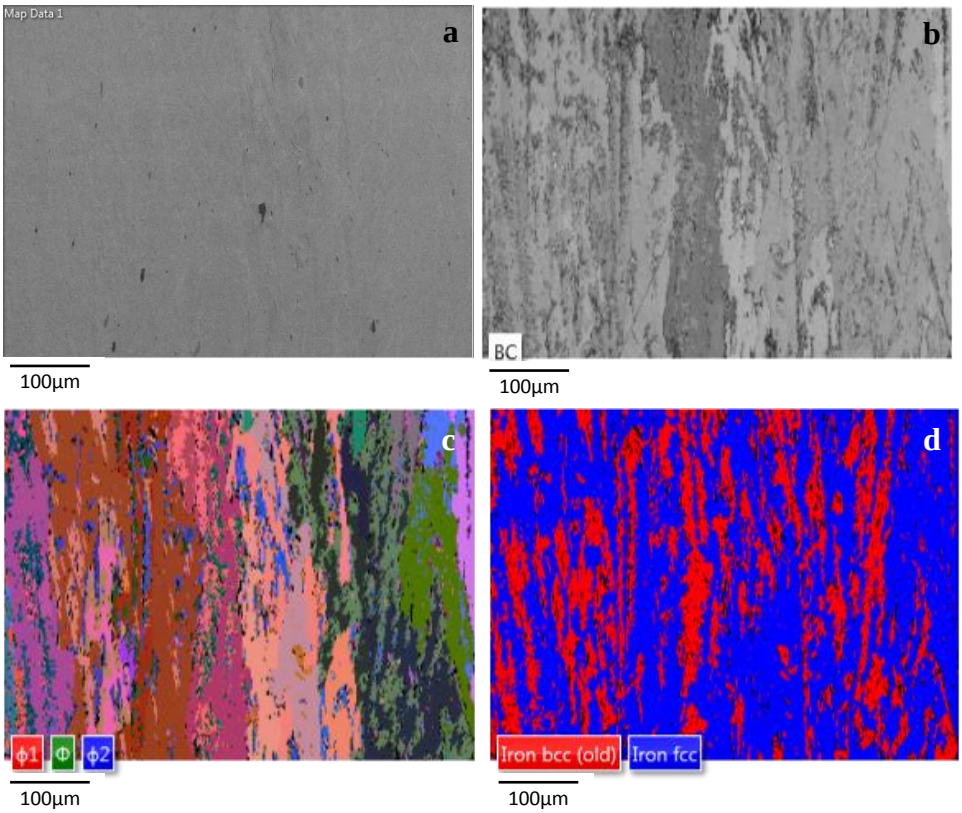

Fig.7: EBSD analysis of weld material close to the border of wrought base material aged for 4000 hours at 750°C. (a) SEM image, (b) band contrast, (c) Euler colour, (d) phase distribution.

Conclusions

This paper has studied the phase distribution and transformations of autogenous weld metal between 321 austenitic stainless steel and a Nb stabilised stainless steel up to 4000 hours ageing at 750°C. The results showed that the weld remained fully austenitic with no noticeable transformations happened in the material until 1000 hours of ageing, which was expected. At 1000 hours and up to 4000 hours ageing, a large scale BCC transformation begins to take place at the boundaries to the base materials. This transformation appears displacive, due to the lack of alloying elements diffusing into the newly transformed ferrite. However the lack of transformation towards the middle of the weld area suggests that there is diffusion from the base materials involved whereby certain alloying elements are making this type of transformation possible.

The displacively formed ferrite takes different appearances on each side of the weld, with the cast side of the weld taking spheroidal regions of BCC phase, and the wrought side of the weld having long, columnar transformations of BCC material. This is despite there being columnar weld grains in the cast side of the weld. This will be due to the difference of diffusion from each alloy.

Acknowledgements

The authors would like to thank EDF energy for supplying the material for this study.

Thanks also go to EDF Energy and the ESPRC for funding this work.

References

[1] Department of Energy and Climate Change, Maintaining UK energy security, London. 2013.

[2] Abe F, Torsten-Ulf Kern, R.Viswanathan. Creep Resistant Steels. Cambridge: Woodhead publishing; 2008.

[3] ASTM. ASTM 312 / A312M - Standard Specification for Seamless , Welded , and Heavily Cold Worked Austenitic Stainless Steel Pipes, 2014.

[4] T. Sourmail, Sourmail T. Precipitation in Creep Resistant Austenitic Stainless Steels. IoM Commun 2001;17:1–14.

[5] Callister WD. Materials Science And Engineering: An Introduction. vol. 57. John Wiley & Sons; 2007.

[6] John V. Introduction to Engineering Materials. 3rd ed. Basingstoke: Palgrave Macmillan; 2003.

[7] Newey C, Weaver G. Materials Principles and Practice. The Open University: Butterworths; 1990.

[8] Guan K, Xu X, Xu H, Wang Z. Effect of aging at 700°C on precipitation and toughness of AISI 321 and AISI 347 austenitic stainless steel welds. Nucl Eng Des 2005;235:2485–94.

[9] Senior BA. The solidification and in-service transformation behaviour of type 316 and 347 welds fabricated with type 321 plate. Mater Sci Eng 1988;100:219–27.

[10] Guan KS, Xu XD, Zhang YY, Wang ZW. Cracks and precipitate phases in 321 stainless steel weld of flue gas pipe. Eng Fail Anal 2005;12:623–33.

[11] Onizawa T, Wakai T, Ando M, Aoto K. Effect of V and Nb on precipitation behavior and mechanical properties of high Cr steel. Nucl Eng Des 2008;238:408–16.

[12] Caminada S, Cumino G, Cipolla L, Venditti D, Di Gianfrancesco A, Minami Y. Creep properties and microstructural evolution of austenitic TEMPALOY steels. Int J Press Vessel Pip 2010;87:336–44.

[13] Danielsen HK, Hald J. Behaviour of Z phase in 9–12%Cr steels. Energy Mater 2006;1:49–57. doi:10.1179/174892306X99732.

[14] Danielsen HK, Hald J. On the nucleation and dissolution process of Z-phase Cr(V,Nb)N in martensitic 12%Cr steels. Mater Sci Eng A 2009;505:169–77.

[15] Cao J, Gong Y, Yang Z-G. Microstructural analysis on creep properties of dissimilar materials joints between T92 martensitic and HR3C austenitic steels. Mater Sci Eng A 2011;528:6103–11.

[16] Lewis M., Hattersley B. Precipitation of M23C6 in austenitic steels. Acta Metall 1965;13:1159–68. doi:10.1016/0001-6160(65)90053-2.

[17] Sinha AK, Moore JJ. Precipitation of M23C6 Carbides in an Aged Inconel X-750 1986;98:87–98.

[18] Carolan RA, Faulkner RG. Grain boundary precipitation of M23C6 in an austenitic steel. Acta Metall 1988;36:257–66. doi:10.1016/0001-6160(88)90002-8.

[19] Lewis M. Precipitation of (Fe, Cr) sigma phase from austenite. Acta Metall 1966;14:1421–8. doi:10.1016/0001-6160(66)90162-3.

[20] Green G, Higginson R, Hogg S, Spindler S, Hamm C. Evolution of sigma phase in 321 grade austenitic stainless steel parent and weld metal with duplex microstructure. Mater Sci Technol 2013:1743284713Y.000. doi:10.1179/1743284713Y.0000000452.

[21] DeLong WT, Long CJ. The Ferrite Content of Austenitic Stainless Steel Weld Metal. Weld Res Suppl 1973.

[22] Pope AM, de Carvalho Mota AF, Monteiro SN, da Silveira TL, le May I. Aging and mechanical behavior of type 304/347 welded joints. Metallography 1981;14:141–50.

[23] Chi C, Yu H, Dong J, Liu W, Cheng S, Liu Z, et al. The precipitation strengthening behavior of Cu-rich phase in Nb contained advanced Fe–Cr–Ni type austenitic heat resistant steel for USC power plant application. Prog Nat Sci Mater Int 2012;22:175–85. doi:10.1016/j.pnsc.2012.05.002.

[24] Green G, Higginson R, Hogg S, Spindler S, Hamm C, Najorka J. Analysis of ferrite formed in 321 grade austenitic stainless steel. Mater Sci Technol 2014:1743284714Y.000. doi:10.1179/1743284714Y.0000000564.